

Single-gap isotropic s -wave superconductivity in single crystals AuSn_4

Sunil Ghimire^{1,2}, Kamal R. Joshi^{1,2}, Elizabeth H. Krenkel^{1,2}, Makariy A. Tanatar^{1,2},
Marcin Kończykowski³, Romain Grasset³, Paul C. Canfield^{1,2} and Ruslan Prozorov^{1,2*}

¹ Ames National Laboratory, Ames, Iowa 50011, USA

² Department of Physics & Astronomy, Iowa State University, Ames, Iowa 50011, USA

³ Laboratoire des Solides Irradiés, CEA/DRF/IRAMIS, École Polytechnique,
CNRS, Institut Polytechnique de Paris, F-91128 Palaiseau, France

* prozorov@ameslab.gov

Abstract

London, $\lambda_L(T)$, and Campbell, $\lambda_C(T)$, penetration depths were measured in single crystals of a topological superconductor candidate AuSn_4 . At low temperatures, $\lambda_L(T)$ is exponentially attenuated and, if fitted with the power law, $\lambda(T) \sim T^n$, gives exponents $n > 4$, indistinguishable from the isotropic single s -wave gap Bardeen-Cooper-Schrieffer (BCS) asymptotic. The superfluid density fits perfectly in the entire temperature range to the BCS theory. The superconducting transition temperature, $T_c = 2.40 \pm 0.05$ K, does not change after 2.5 MeV electron irradiation, indicating the validity of the Anderson theorem for isotropic s -wave superconductors. Campbell penetration depth before and after electron irradiation shows no hysteresis between the zero-field cooling (ZFC) and field cooling (FC) protocols, consistent with the parabolic pinning potential. Interestingly, the critical current density estimated from the original Campbell theory decreases after irradiation, implying that a more sophisticated theory involving collective effects is needed to describe vortex pinning in this system. In general, our thermodynamic measurements strongly suggest that the bulk response of the AuSn_4 crystals is fully consistent with the isotropic s -wave weak-coupling BCS superconductivity.



Copyright S. Ghimire *et al.*

This work is licensed under the Creative Commons

[Attribution 4.0 International License](https://creativecommons.org/licenses/by/4.0/).

Published by the SciPost Foundation.

Received 04-07-2024

Accepted 08-10-2024

Published 21-10-2024

doi:[10.21468/SciPostPhys.17.4.116](https://doi.org/10.21468/SciPostPhys.17.4.116)



Check for
updates

Contents

1	Introduction	2
2	Samples and methods	2
3	Results	3
3.1	London penetration depth	3
3.2	Campbell penetration depth	6
4	Conclusions	8
	References	8

1 Introduction

In recent years, superconductors with topological features in their electronic bandstructure have attracted significant interest for various novel features predicted by a well-developed theory, for example, emerging zero-energy excitations called Majorana fermions [1]. On the material side, the search for topological superconductors (TSCs) is very active but so far has yielded only a few “candidates” whose topological properties have not yet been fully confirmed experimentally, including UTe_2 [2], Sr_2RuO_4 [3–5], UPt_3 [6], 2M-WS_2 [7], and $\text{M}_x\text{Bi}_2\text{Se}_3$ with $\text{M}=\text{Cu}$ [8, 9]. The subject of this study, AuSn_4 , is another promising TSC candidate with theoretically predicted non-trivial topological characteristics [10–13].

The superconductivity in orthorhombic AuSn_4 with a transition temperature to the superconducting state, $T_c = 2.4$ K, was discovered in 1962 [14]. This compound is isostructural to PtSn_4 [15] and PdSn_4 [16], which are not superconductors. The first principal study suggests semimetallic behavior with type I nodes [12]. The magneto-transport measurements show two-dimensional (2D) superconductivity in AuSn_4 [11, 17]. Recently, ARPES measurements supported by DFT calculations [13] revealed nearly degenerate polytypes in AuSn_4 crystals, making it a unique case of a three-dimensional (3D) electronic band structure with properties of a low-dimensional layered material. Thermodynamic magnetization and specific heat measurement in AuSn_4 single crystals are consistent with conventional nodeless s -wave Bardeen-Cooper-Schrieffer (BCS) [18, 19] superconductivity [11]. Scanning tunneling microscopy (STM) measurements determined the superconducting gap to T_c ratio close to the s -wave BCS value of $\Delta/T_c = 1.76$ [13]. However, other STM measurements suggest unconventional 2D superconductivity with a mixture of p -wave surface states and s -wave bulk [10]. Clearly, more measurements are required for an objective and conclusive determination of the nature of superconductivity in AuSn_4 .

Here, we probe the bulk nature of superconductivity in AuSn_4 single crystals by measuring London and Campbell penetration depths using a highly sensitive tunnel-diode resonator (TDR). Furthermore, we examine the response to a controlled non-magnetic point-like disorder induced by 2.5 MeV electron irradiation. We conclude that AuSn_4 is a robust isotropic s -wave superconductor in the bulk. However, we cannot exclude the possibility that it could have a different type of superconductivity in the surface atomic layers, where the STM is most sensitive.

2 Samples and methods

Single crystals of AuSn_4 were grown with excess Sn flux [13, 20, 21]. High-purity Au and Sn were mixed in a 12:88 ratio in a fritted crucible [22, 23] and sealed in a quartz ampoule under an Ar gas atmosphere. The ampoule was heated to 1100 °C over 12 hours, then cooled to 250 °C in 12 hours, and significantly slower to 230 °C over 90 hours. The ampoule was held at this temperature for 48 hours prior to removal from the furnace.

The London penetration depth, $\lambda(T)$, was measured using a sensitive frequency-domain self-oscillating tunnel-diode resonator (TDR) operating at a frequency of around 14 MHz. Measurements were performed in a ^3He cryostat with a base temperature of ≈ 400 mK, which is $0.17T_c$, allowing us to examine the low-temperature limit, which starts below approximately $T_c/3$, below which the superconducting gap is approximately constant [19]. The experimental setup, measurement protocols, and calibration are described in detail elsewhere [24–28].

Briefly, the sample placed inside the inductor of the LC -tank circuit affects the total inductance, L , leading to a shift of its resonant frequency, $2\pi f = 1/\sqrt{LC}$ by the amount proportional to the magnetic susceptibility of the sample, $\Delta f = G\chi(T)$, where G is the cali-

bration constant [25,27]. A small excitation magnetic field of the setup, $\sim 20\text{mOe}$, ensures the regime of a small-amplitude linear magnetic response where $\chi = \lambda_m/R \tanh(R/\lambda_m) - 1$. Here R is the effective dimension of the sample and λ_m is the total measured magnetic penetration depth [27]. The sample of this study had dimensions $0.6 \times 0.4 \times 0.1 \text{ mm}^3$, which gives the effective dimension $R = 84.1 \mu\text{m}$, calculated using the procedure described in Ref. [27]. With a penetration depth smaller than a few micrometers for most of the temperature range, we can simplify the relation for magnetic susceptibility to $\chi \approx \lambda_m/R - 1$. Therefore, the change in $\lambda_m(T)$ with respect to a reference point at the lowest temperature, $\lambda_m(T_{min})$ is proportional to the relative frequency shift, $\Delta\lambda_m(T) = \lambda_m(T) - \lambda_m(0.4 \text{ K}) = (R/G)\Delta f$. For all practical purposes, $\lambda_m(0) \approx \lambda_m(0.4 \text{ K})$. Although the calibration constant G can be calculated, in our setup it is measured directly by mechanically extracting the sample from the coil at low temperature, thus providing a robust calibration specific for each sample studied.

In a zero magnetic field, there are no vortices and the measured penetration depth is the London penetration depth, $\lambda_L(T)$. Therefore, by measuring the change, $\Delta\lambda_L(T) = \lambda_m(T, B=0)$, and adding the absolute value, $\lambda(0)$ determined from other measurements, such as fitting $\Delta\lambda(T)$ in Fig.2, a full London length is obtained, $\lambda_L(T) = \lambda_L(0) + \Delta\lambda_L(T)$. In the presence of a magnetic field, in a small-amplitude linear AC response, the vortex-mediated Campbell length adds to the London length, $\lambda_m^2 = \lambda_C^2 + \lambda_L^2$ [29–31]. Upon approaching the transition temperature, T_c , the penetration depth can only increase up to a normal-metal skin depth. Since the magnetoresistance at T_c is known and in this case is negligible, the value at T_c is used as a fixed reference point [13]. Measuring $\lambda_m(T, B)$ in finite magnetic fields, the curves are shifted vertically, so that the saturation flat parts above T_c match. Once such a vertical shift procedure is performed, the full Campbell penetration depth is extracted from $\lambda_C = \sqrt{\lambda_m^2 - \lambda_L^2}$.

Point-like disorder was introduced at the SIRIUS facility in the Laboratoire des Solides Irradiés at École Polytechnique in Palaiseau, France. Electrons, accelerated in a pelletron-type linear accelerator to 2.5 MeV, knock out ions, creating vacancy-interstitial Frenkel pairs [32,33]. During irradiation, the sample is immersed in liquid hydrogen at around 20 K. This ensures efficient heat removal upon impact and prevents immediate recombination and migration of the produced atomic defects. The acquired irradiation dose is determined by measuring the total charge collected by a Faraday cage located behind the sample. As such, the acquired dose is measured in the “natural” units of C/cm^2 , which is equal to $1\text{C}/\text{cm}^2 \equiv 1/e \approx 6.24 \times 10^{18}$ electrons per cm^2 . Upon warming to room temperature, some defects recombine, and some migrate to various sinks (dislocations, surfaces, etc.). This leaves a metastable population, about 70%, of point-like defects [34,35]. Importantly, the same sample has been measured before and after electron irradiation.

3 Results

3.1 London penetration depth

Figure 1 shows the low-temperature dependence of the change in the London penetration depth, $\Delta\lambda(T) = \lambda(T) - \lambda(T_{min} = 0.4 \text{ K})$ before (blue circles) and after $2.5 \text{ C}/\text{cm}^2$ electron irradiation (red circles). The upper left inset shows the exponent n determined from the power-law fitting, $\Delta\lambda(T) \sim At^n$, as a function of the upper fitting limit, $t_{max} = T_{max}/T_c$. The solid lines in the main frame show an example of such a fitting with $t_{max} = 0.4$. The results show a robust and consistent behavior with $n \geq 4$, indicating experimentally indistinguishable from the exponential temperature dependence. The exponent, n , decreased after irradiation as it should be in an s -wave superconductor [36,37].

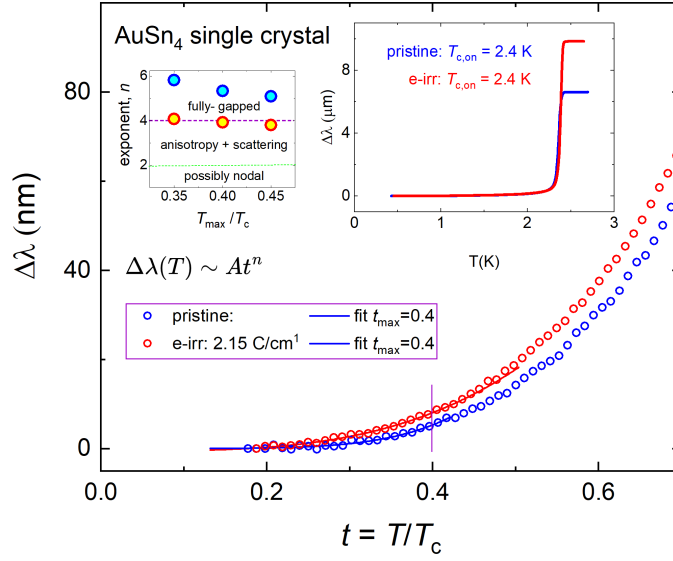


Figure 1: Main Panel: Low-temperature temperature variation of the London penetration depth $\Delta\lambda(T) = \lambda(T) - \lambda(0.4 \text{ K})$ as a function of normalized temperature, $t = T/T_c$, for pristine (blue circles) and irradiated at 2.5 C/cm^2 (red circles) single crystal of AuSn_4 . Lines show fits to the power law, $\Delta\lambda(T) \sim At^n$, with the upper range of $t_{max} = 0.4$. The top right inset shows the $\Delta\lambda(T)$ in the whole temperature range, showing sharp superconducting transition with onset $T_c = 2.4 \text{ K}$ for both pristine and electron irradiated state. The top left inset shows the exponent n versus the upper limit of the power-law fitting, $t_{max} = T_{max}/T_c$, indicating robustness of the power law, experimentally indistinguishable from exponential.

The upper right inset of Fig.1 shows $\Delta\lambda(T)$ of the same sample in its pristine state and after 2.15 C/cm^2 electron irradiation as a function of absolute temperature T . One might think that for some reason (e.g., defect annealing and recombination), there was no increase in disorder after irradiation. It is straightforward to prove that this is not the case. The saturation of the measured $\lambda(T)$ above T_c occurs when it reaches the skin depth of the normal state, $\delta_{skin} = \sqrt{\rho/\mu_0\pi f}$, where $\mu_0 = 4\pi \times 10^{-7} \text{ H/m}$ is the vacuum permeability, and ρ is the resistance. More precisely, $\delta_{skin}(T_c) = 2\lambda(T_c)$ [38]. We did not measure resistivity in this particular AuSn_4 sample, but we directly compared resistivity from transport measurements and extracted from the skin depth on the same samples of other compounds and always found good quantitative agreement [39, 40]. Furthermore, the upper critical fields are small, $H_{c2}^{||ab} = 130 \text{ Oe}$ and $H_{c2}^{||c} = 90 \text{ Oe}$ [11]. Consulting with published magnetoresistance [13], we find that the expected variation of δ_{skin} just above T_c is negligible. On the other hand, the top right inset in Fig.1 shows a substantial increase in saturation value after electron irradiation. This proves a substantial increase of resistivity, which can only be due to added disorder scattering. Therefore, the fact that the superconducting transition temperature T_c remains unchanged is consistent with the Anderson theorem for isotropic s -wave superconductors [41, 42]. We have observed similar robust superconductivity in another low- T_c superconductor with non-trivial topology, LaNiGa_2 [43].

The exponential temperature dependence of $\lambda(T)$ can be fitted with the well-known low-temperature asymptotic BCS, $\Delta\lambda(T) = \lambda(0)\sqrt{\frac{\pi\delta}{2t}}e^{-\frac{\delta}{t}}$ [19], where the ratio $\delta = \Delta(0)/T_c$ was fixed at $\delta \approx 1.764$, leaving only one free parameter $\lambda(0)$. The fitting is shown in the top panel of Fig.2. It produces $\lambda(0) = 150 \text{ nm}$ in the pristine state (blue fitting curve and blue data symbols) and $\lambda(0) = 258 \text{ nm}$ after 2.15 C/cm^2 electron irradiation (red curve and symbols).

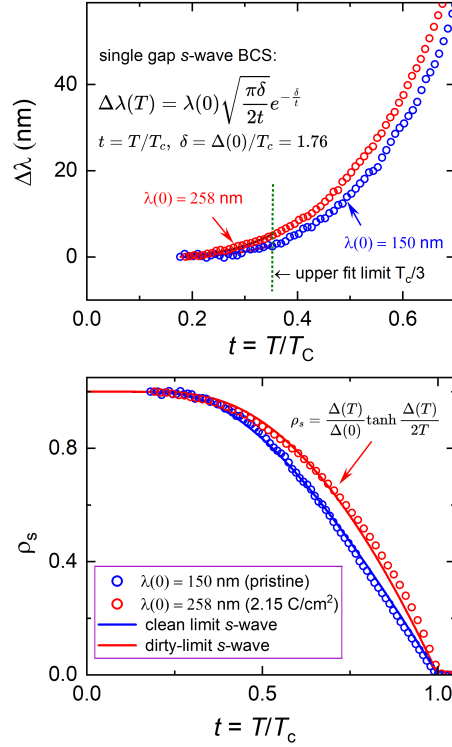


Figure 2: Top panel. Fit to the BCS low-temperature asymptotic, $\Delta\lambda(T) = \lambda(0)\sqrt{\frac{\pi\delta}{2t}}e^{-\frac{\delta}{t}}$ with a fixed ratio $\delta = \Delta(0)/T_c \approx 1.76$ leaving only one free parameter, $\lambda(0) = 150 \text{ nm}$ in the pristine sample (blue fitting curve and blue data symbols) and $\lambda(0) = 258 \text{ nm}$ after 2.15 C/cm^2 electron irradiation (red curve and symbols). Bottom panel: Superfluid density calculated from the data, $\rho_s(T) = (1 + \Delta\lambda(T)/\lambda(0))^{-2}$. Solid lines show self-consistent full temperature range calculations using Eilenberger formalism for pristine (blue line) and irradiated (red line) states. The known analytical expression for the s-wave dirty limit is shown in [44].

With these numbers, we can calculate the superfluid density in the full temperature range using $\rho_s(T) \equiv (\lambda(0)/\lambda(T))^2 = (1 + \Delta\lambda(T)/\lambda(0))^{-2}$. The bottom panel of Fig.2 shows $\rho_s(T)$ by blue and red circles for the pristine and irradiated states of the same sample, respectively. The theoretical lines of the clean (blue) and dirty (red) limits were calculated self-consistently using the Eilenberger formalism [45]. The analytical dirty limit formula, $\rho_s = (\Delta(T)/\Delta(0)) \tanh(\Delta(T)/2T)$ reproduces the numerical calculation precisely [44]. We note that due to a limited number of data points, good fits of $\lambda(T)$ can also be obtained with slightly different ratios of $\Delta(0)/T_c$. However, then the full-range superfluid density curve does not fit. It fits only with the weak-coupling isotropic BCS value of 1.764. In summary, Fig.2 shows that the classical BCS theory describes the experimental data well.

To summarize our findings from measurements of the London penetration depth, $\lambda(T)$, several independent characteristics: (1) low-temperature behavior of $\lambda(T)$; (2) full temperature range behavior of ρ_s ; (3) disorder-independent T_c before and after electron irradiation, fully agree with the BCS theory for the isotropic s-wave gap with the ratio $\delta = \Delta(0)/T_c \approx 1.76$. This is the nature of superconductivity in the bulk of AuSn₄ crystals. However, our measurements would not pick up a tiny signal coming from the surface atomic layers, so unconventional topological features are still possible.

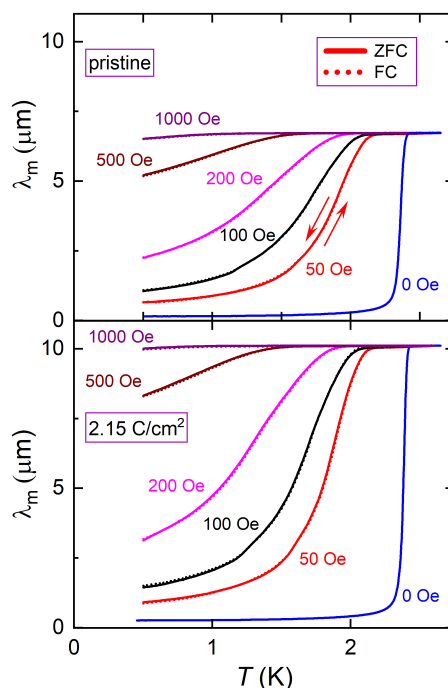


Figure 3: Temperature variation of the measured magnetic penetration depth, λ_m , before (top panel) and after (bottom panel) electron irradiation, measured with the various dc magnetic fields applied along the c - axis. The field values are shown. Solid lines correspond to zero-field cooling (ZFC), and dotted lines correspond to field cooling (FC) protocols. For one curve, this is shown by arrows. The ZFC and FC curves are indistinguishable, implying that the process is completely reversible, indicating the pinning potential's parabolic shape. Note that the axes scales are the same in the top and bottom panels, aiding in a visual comparison of the effect of irradiation.

3.2 Campbell penetration depth

The temperature variation of the magnetic penetration depth before (top panel) and after (bottom panel) electron irradiation, measured in various dc magnetic fields applied along the c - axis, is shown in Fig.3. The field values are shown next to each curve. Solid lines correspond to zero-field cooling (ZFC) in all curves, and dotted lines correspond to field cooling (FC) protocols. For one curve, this is shown by arrows. The ZFC and FC curves are indistinguishable, implying that the process is totally reversible, which indicates a parabolic shape of the pinning potential.

In the presence of an external DC magnetic field, Abrikosov vortices penetrate the sample and form a vortex lattice. Then the measured penetration depth, λ_m , has two contributions, the usual London penetration depth that in this section we explicitly denote as λ_L , and the Campbell penetration depth λ_C , which is a characteristic length scale over which a small ac perturbation is transmitted elastically by a vortex lattice into the sample [46–49]. More specifically, the amplitude of the ac perturbation must be small enough so that the vortices remain in their potential well, and their motion is described by the reversible linear elastic response. In this case, $\lambda_m^2 = \lambda_L^2 + \lambda_C^2$ [29, 50]. This requirement of a very small amplitude makes most conventional ac susceptibility techniques inapplicable for the measurements of the Campbell length. Specialized frequency domain resonators with sufficient sensitivity to a small excitation ac magnetic field are needed [51, 52]. Until now, only a few experimental studies have been published [31, 51–54].

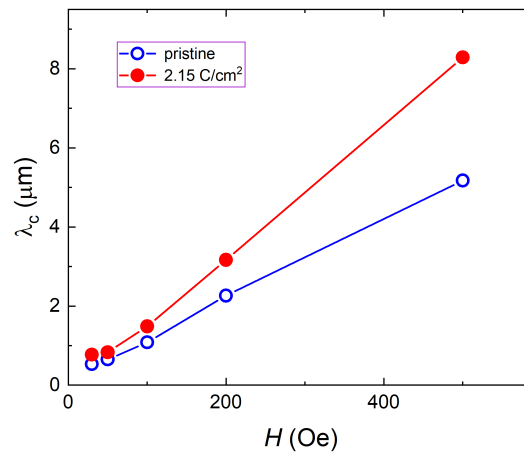


Figure 4: Campbell penetration depth, $\lambda_c^2 = \sqrt{\lambda_m^2 - \lambda_L^2}$ as a function of an applied magnetic field, H , evaluated from the data shown in Fig. 3 at a fixed temperature of $T = 0.5$ K, for a FC protocol comparing pristine (blue symbols) and irradiated (red symbols) states of the same sample.

Figure 3 shows the temperature-dependent variation of the magnetic penetration depth, $\lambda_m(T) = \lambda_L(0) + \Delta\lambda_m(T)$, for different values of the dc magnetic field applied parallel to the sample c -axis. For $\lambda_L(0)$, we have used the values obtained from the BCS fit; see the upper panel of Fig. 2. Then, we assumed that, above T_c , the resistivity is field independent, so we adjusted other curves to match that value. The top panel shows a pristine state, and the bottom panel shows the same sample after electron irradiation.

Generally speaking, the Campbell penetration depth can exhibit a hysteresis upon warming and cooling, indicating an anharmonic (non-parabolic) pinning potential and/or strong pinning [49, 51, 54, 55]. Therefore, there are two types of measurement protocols: zero-field cooling (ZFC) and field cooling (FC). In the ZFC protocol, the Campbell length is measured on warming after the sample was cooled in a zero magnetic field and the target field was applied at the base temperature (solid lines in Fig. 3). In the FC protocol, measurements are performed on cooling in a target magnetic field applied above T_c (dotted lines in Fig. 3). For both pristine and irradiated states, $\lambda_m(T)$ shows a monotonic increase with temperature, and there is no hysteresis between the ZFC and FC protocols. To aid in visualizing the effect of irradiation, the scales of the axes in Fig. 3 are the same in the top and bottom panels. It is clear that the measured penetration depth has increased after electron irradiation.

Figure 4 shows the Campbell penetration depth as a function of an applied magnetic field, H , evaluated from the data shown in Fig. 3 at a fixed temperature of $T = 0.5$ K for a FC protocol comparing pristine (blue symbols) and irradiated (red symbols) states of the same sample. The Campbell length λ_c increases after electron irradiation. In the simple Campbell model [46, 47], $\lambda_c^2 = \phi_0 H / \alpha$, where ϕ_0 is the magnetic flux quantum and α is the curvature of the pinning potential, $\alpha = d^2U/dr^2$. The critical current density $j_c = \alpha r_p / \phi_0 = H r_p / \lambda_c^2$, where r_p is the radius of the pinning potential, usually assumed to be of the order of the coherence length, ξ . We note that this critical current is not the same as the persistent current obtained in conventional magnetization measurements, which is based on the Bean model that assumes a constant vortex density gradient [56, 57]. In the present measurements, the critical current is a parameter of the model defining the equilibrium Campbell length without persistent Bean currents present. It represents a theoretical current density supported by a specific pinning potential, $U(r)$. The conventional measured current density is lower due to magnetic relaxation, which is very fast on short time scales and later slows down to become time-logarithmic [58].

In a more general picture, α is determined by the elementary pinning forces [48, 49, 59]. In the original model with a fixed r_p , the Campbell length is expected to scale as $\lambda_C \sim \sqrt{H}$, but Fig. 4 shows a practically linear temperature dependence, especially after irradiation. This indicates that vortex pinning in AuSn₄ is more complicated with a field-dependent radius of the pinning potential, which is possible, for example, in a collective pinning theory when the vortex lattice evolves from the single-vortex pinning regime to the vortex bundle regime [58]. In addition, it is known that the coherence length increases with the magnetic field [60]. Therefore, if $\xi \sim H$, then λ_C will be a linear function of the applied field. As for the difference between pristine and irradiated states, it is possible that the collective pinning in the pristine state is replaced by the disordered vortex phase after electron irradiation, and one cannot directly compare the critical current densities using the same formula. In any case, the nature of pinning in AuSn₄ requires further investigation.

4 Conclusions

We report measurements of London, $\lambda_L(T)$, and Campbell, $\lambda_C(T)$, penetration depths in single crystals of the topological superconductor candidate AuSn₄ to elucidate the nature of superconductivity in the bulk. Several independent parameters studied before and after 2.5 MeV electron irradiation unambiguously point to isotropic single *s*-wave gap weak coupling BCS superconductor. Specifically, the superfluid density before and after electron irradiation overlaps almost perfectly with the parameter-free theoretical BCS curves in the full temperature range for clean and dirty limits, respectively. The Campbell penetration depth before and after electron irradiation does not show hysteresis between the ZFC and FC data, indicating a parabolic shape of the pinning potential. However, the *H*-linear behavior of λ_C implies either the field-dependent Labusch parameter, α , or the radius of the pinning potential, r_p , or both. Considering the low pinning in AuSn₄ single crystals and the point-like nature of the induced defects, such a field dependence may be expected in the vortex bundle regimes within the collective pinning theory [58].

Acknowledgments

We thank Hermann Suderow for fruitful discussions.

Funding information This work was supported by the US DOE, Office of Science, BES Materials Science and Engineering Division under the contract # DE-AC02-07CH11358. The authors acknowledge support from the EMIRA French network (FR CNRS 3618) on the SIRIUS platform.

References

- [1] C. Nayak, S. H. Simon, A. Stern, M. Freedman and S. Das Sarma, *Non-Abelian anyons and topological quantum computation*, Rev. Mod. Phys. **80**, 1083 (2008), doi:[10.1103/RevModPhys.80.1083](https://doi.org/10.1103/RevModPhys.80.1083).
- [2] S. Ran et al., *Nearly ferromagnetic spin-triplet superconductivity*, Science **365**, 684 (2019), doi:[10.1126/science.aav8645](https://doi.org/10.1126/science.aav8645).

- [3] Y. Maeno, S. Kittaka, T. Nomura, S. Yonezawa and K. Ishida, *Evaluation of spin-triplet superconductivity in Sr_2RuO_4* , J. Phys. Soc. Jpn. **81**, 011009 (2012), doi:[10.1143/jpsj.81.011009](https://doi.org/10.1143/jpsj.81.011009).
- [4] C. Kallin and A. J. Berlinsky, *Is Sr_2RuO_4 a chiral p -wave superconductor?*, J. Phys.: Condens. Matter **21**, 164210 (2009), doi:[10.1088/0953-8984/21/16/164210](https://doi.org/10.1088/0953-8984/21/16/164210).
- [5] C. Kallin, *Chiral p -wave order in Sr_2RuO_4* , Rep. Prog. Phys. **75**, 042501 (2012), doi:[10.1088/0034-4885/75/4/042501](https://doi.org/10.1088/0034-4885/75/4/042501).
- [6] R. Joynt and L. Taillefer, *The superconducting phases of UPt_3* , Rev. Mod. Phys. **74**, 235 (2002), doi:[10.1103/RevModPhys.74.235](https://doi.org/10.1103/RevModPhys.74.235).
- [7] Y. Fang et al., *Discovery of superconductivity in $2M WS_2$ with possible topological surface states*, Adv. Mater. **31**, 1901942 (2019), doi:[10.1002/adma.201901942](https://doi.org/10.1002/adma.201901942).
- [8] L. Fu and E. Berg, *Odd-parity topological superconductors: Theory and application to $Cu_xBi_2Se_3$* , Phys. Rev. Lett. **105**, 097001 (2010), doi:[10.1103/PhysRevLett.105.097001](https://doi.org/10.1103/PhysRevLett.105.097001).
- [9] Y. S. Hor et al., *Superconductivity in $Cu_xBi_2Se_3$ and its implications for pairing in the undoped topological insulator*, Phys. Rev. Lett. **104**, 057001 (2010), doi:[10.1103/PhysRevLett.104.057001](https://doi.org/10.1103/PhysRevLett.104.057001).
- [10] W. Zhu et al., *Intrinsic surface p -wave superconductivity in layered $AuSn_4$* , Nat. Commun. **14**, 7012 (2023), doi:[10.1038/s41467-023-42781-7](https://doi.org/10.1038/s41467-023-42781-7).
- [11] D. Shen, C. N. Kuo, T. W. Yang, I. N. Chen, C. S. Lue and L. M. Wang, *Two-dimensional superconductivity and magnetotransport from topological surface states in $AuSn_4$ semimetal*, Commun. Mater. **1**, 56 (2020), doi:[10.1038/s43246-020-00060-8](https://doi.org/10.1038/s43246-020-00060-8).
- [12] N. K. Karn, M. M. Sharma and V. P. S. Awana, *Non-trivial band topology in the superconductor $AuSn_4$: A first principle study*, Supercond. Sci. Technol. **35**, 114002 (2022), doi:[10.1088/1361-6668/ac9160](https://doi.org/10.1088/1361-6668/ac9160).
- [13] E. Herrera et al., *Band structure, superconductivity, and polytypism in $AuSn_4$* , Phys. Rev. Mater. **7**, 024804 (2023), doi:[10.1103/PhysRevMaterials.7.024804](https://doi.org/10.1103/PhysRevMaterials.7.024804).
- [14] M. F. Gendron and R. E. Jones, *Superconductivity in the $CuAl_2$ ($C16$) crystal class*, J. Phys. Chem. Solids **23**, 405 (1962), doi:[10.1016/0022-3697\(62\)90107-5](https://doi.org/10.1016/0022-3697(62)90107-5).
- [15] Y. Wu et al., *Dirac node arcs in $PtSn_4$* , Nat. Phys. **12**, 667 (2016), doi:[10.1038/nphys3712](https://doi.org/10.1038/nphys3712).
- [16] N. H. Jo et al., *Extremely large magnetoresistance and Kohler's rule in $PdSn_4$: A complete study of thermodynamic, transport, and band-structure properties*, Phys. Rev. B **96**, 165145 (2017), doi:[10.1103/PhysRevB.96.165145](https://doi.org/10.1103/PhysRevB.96.165145).
- [17] M. M. Sharma, G. Gurjar, S. Patnaik and V. P. S. Awana, *Two-fold anisotropic superconducting state in topological superconductor Sn_4Au* , Europhys. Lett. **142**, 26004 (2023), doi:[10.1209/0295-5075/acc8f5](https://doi.org/10.1209/0295-5075/acc8f5).
- [18] J. Bardeen, L. N. Cooper and J. R. Schrieffer, *Microscopic theory of superconductivity*, Phys. Rev. **106**, 162 (1957), doi:[10.1103/physrev.106.162](https://doi.org/10.1103/physrev.106.162).
- [19] J. Bardeen, L. N. Cooper and J. R. Schrieffer, *Theory of superconductivity*, Phys. Rev. **108**, 1175 (1957), doi:[10.1103/PhysRev.108.1175](https://doi.org/10.1103/PhysRev.108.1175).

- [20] H. Okamoto, *Au-Sn (gold-tin)*, J. Ph. Equilibria Diffus. **28**, 490 (2007), doi:[10.1007/s11669-007-9147-1](https://doi.org/10.1007/s11669-007-9147-1).
- [21] P. C. Canfield, *New materials physics*, Rep. Prog. Phys. **83**, 016501 (2019), doi:[10.1088/1361-6633/ab514b](https://doi.org/10.1088/1361-6633/ab514b).
- [22] P. C. Canfield, T. Kong, U. S. Kaluarachchi and N. H. Jo, *Use of frit-disc crucibles for routine and exploratory solution growth of single crystalline samples*, Philos. Mag. **96**, 84 (2016), doi:[10.1080/14786435.2015.1122248](https://doi.org/10.1080/14786435.2015.1122248).
- [23] *Canfield crucible sets*, <https://www.lspceramics.com/canfield-crucible-sets-2>.
- [24] C. T. Van Degrift, *Tunnel diode oscillator for 0.001 ppm measurements at low temperatures*, Rev. Sci. Instrum. **46**, 599 (1975), doi:[10.1063/1.1134272](https://doi.org/10.1063/1.1134272).
- [25] R. Prozorov, R. W. Giannetta, A. Carrington and F. M. Araujo-Moreira, *Meissner-London state in superconductors of rectangular cross section in a perpendicular magnetic field*, Phys. Rev. B **62**, 115 (2000), doi:[10.1103/PhysRevB.62.115](https://doi.org/10.1103/PhysRevB.62.115).
- [26] R. Prozorov, R. W. Giannetta, A. Carrington, P. Fournier, R. L. Greene, P. Guptasarma, D. G. Hinks and A. R. Banks, *Measurements of the absolute value of the penetration depth in high- T_c superconductors using a low- T_c superconductive coating*, Appl. Phys. Lett. **77**, 4202 (2000), doi:[10.1063/1.1328362](https://doi.org/10.1063/1.1328362).
- [27] R. Prozorov, *Meissner-London susceptibility of superconducting right circular cylinders in an axial magnetic field*, Phys. Rev. Appl. **16**, 024014 (2021), doi:[10.1103/physrevapplied.16.024014](https://doi.org/10.1103/physrevapplied.16.024014).
- [28] R. Giannetta, A. Carrington and R. Prozorov, *London penetration depth measurements using tunnel diode resonators*, J. Low Temp. Phys. **208**, 119 (2021), doi:[10.1007/s10909-021-02626-3](https://doi.org/10.1007/s10909-021-02626-3).
- [29] E. H. Brandt, *Penetration of magnetic ac fields into type-II superconductors*, Phys. Rev. Lett. **67**, 2219 (1991), doi:[10.1103/PhysRevLett.67.2219](https://doi.org/10.1103/PhysRevLett.67.2219).
- [30] P. Prommapan, M. A. Tanatar, B. Lee, S. Khim, K. H. Kim and R. Prozorov, *Magnetic-field-dependent pinning potential in LiFeAs superconductor from its Campbell penetration depth*, Phys. Rev. B **84**, 060509 (2011), doi:[10.1103/PhysRevB.84.060509](https://doi.org/10.1103/PhysRevB.84.060509).
- [31] H. Kim, M. A. Tanatar, H. Hodovanets, K. Wang, J. Paglione and R. Prozorov, *Campbell penetration depth in low carrier density superconductor YPtBi*, Phys. Rev. B **104**, 014510 (2021), doi:[10.1103/PhysRevB.104.014510](https://doi.org/10.1103/PhysRevB.104.014510).
- [32] A. C. Damask and G. J. Dienes, *Point defects in metals*, Gordon & Breach, London, UK, ISBN 9780677001906 (1963).
- [33] M. W. Thompson, *Defects and radiation damage in metals*, Cambridge University Press, Cambridge, UK, ISBN 9780521098656 (1974).
- [34] R. Prozorov, M. Kończykowski, M. A. Tanatar, A. Thaler, S. L. Bud'ko, P. C. Canfield, V. Mishra and P. J. Hirschfeld, *Effect of electron irradiation on superconductivity in single crystals of Ba(Fe_{1-x}Ru_x)₂As₂ (x = 0.24)*, Phys. Rev. X **4**, 041032 (2014), doi:[10.1103/PhysRevX.4.041032](https://doi.org/10.1103/PhysRevX.4.041032).

- [35] R. Prozorov, M. Kończykowski, M. A. Tanatar, H.-H. Wen, R. M. Fernandes and P. C. Canfield, *Interplay between superconductivity and itinerant magnetism in underdoped $Ba_{1-x}K_xFe_2As_2$ ($x = 0.2$) probed by the response to controlled point-like disorder*, npj Quantum Mater. **4**, 34 (2019), doi:[10.1038/s41535-019-0171-2](https://doi.org/10.1038/s41535-019-0171-2).
- [36] M. Tinkham, *Introduction to superconductivity*, Dover Publications, Mineola, USA, ISBN 9780486435039 (2004).
- [37] V. G. Kogan, R. Prozorov and V. Mishra, *London penetration depth and pair breaking*, Phys. Rev. B **88**, 224508 (2013), doi:[10.1103/PhysRevB.88.224508](https://doi.org/10.1103/PhysRevB.88.224508).
- [38] R. Prozorov and R. W. Giannetta, *Magnetic penetration depth in unconventional superconductors*, Supercond. Sci. Technol. **19**, R41 (2006), doi:[10.1088/0953-2048/19/8/r01](https://doi.org/10.1088/0953-2048/19/8/r01).
- [39] R. T. Gordon et al., *Unconventional London penetration depth in single-crystal $Ba(Fe_{0.93}Co_{0.07})_2As_2$ superconductors*, Phys. Rev. Lett. **102**, 127004 (2009), doi:[10.1103/PhysRevLett.102.127004](https://doi.org/10.1103/PhysRevLett.102.127004).
- [40] H. Kim, M. A. Tanatar, Y. J. Song, Y. S. Kwon and R. Prozorov, *Nodeless two-gap superconducting state in single crystals of the stoichiometric iron pnictide LiFeAs*, Phys. Rev. B **83**, 100502 (2011), doi:[10.1103/PhysRevB.83.100502](https://doi.org/10.1103/PhysRevB.83.100502).
- [41] E. I. Timmons et al., *Electron irradiation effects on superconductivity in $PdTe_2$: An application of a generalized Anderson theorem*, Phys. Rev. Res. **2**, 023140 (2020), doi:[10.1103/PhysRevResearch.2.023140](https://doi.org/10.1103/PhysRevResearch.2.023140).
- [42] P. W. Anderson, *Theory of dirty superconductors*, J. Phys. Chem. Solids **11**, 26 (1959), doi:[10.1016/0022-3697\(59\)90036-8](https://doi.org/10.1016/0022-3697(59)90036-8).
- [43] S. Ghimire et al., *Electron irradiation reveals robust fully gapped superconductivity in $LaNiGa_2$* , Phys. Rev. B **109**, 024515 (2024), doi:[10.1103/PhysRevB.109.024515](https://doi.org/10.1103/PhysRevB.109.024515).
- [44] V. G. Kogan, *Homes scaling and BCS*, Phys. Rev. B **87**, 220507 (2013), doi:[10.1103/PhysRevB.87.220507](https://doi.org/10.1103/PhysRevB.87.220507).
- [45] G. Eilenberger, *Transformation of Gorkov's equation for type II superconductors into transport-like equations*, Z. Phys. A: Hadrons Nucl. **214**, 195 (1968), doi:[10.1007/bf01379803](https://doi.org/10.1007/bf01379803).
- [46] A. M. Campbell, *The response of pinned flux vortices to low-frequency fields*, J. Phys. C: Solid State Phys. **2**, 1492 (1969), doi:[10.1088/0022-3719/2/8/318](https://doi.org/10.1088/0022-3719/2/8/318).
- [47] A. M. Campbell, *The interaction distance between flux lines and pinning centres*, J. Phys. C: Solid State Phys. **4**, 3186 (1971), doi:[10.1088/0022-3719/4/18/023](https://doi.org/10.1088/0022-3719/4/18/023).
- [48] R. Willa, V. B. Geshkenbein and G. Blatter, *Campbell penetration in the critical state of type-II superconductors*, Phys. Rev. B **92**, 134501 (2015), doi:[10.1103/PhysRevB.92.134501](https://doi.org/10.1103/PhysRevB.92.134501).
- [49] F. Gaggioli, G. Blatter and V. B. Geshkenbein, *Creep effects on the Campbell response in type-II superconductors*, Phys. Rev. Res. **4**, 013143 (2022), doi:[10.1103/PhysRevResearch.4.013143](https://doi.org/10.1103/PhysRevResearch.4.013143).
- [50] A. E. Koshelev and V. M. Vinokur, *Frequency response of pinned vortex lattice*, Phys. C: Supercond. **173**, 465 (1991), doi:[10.1016/0921-4534\(91\)90749-o](https://doi.org/10.1016/0921-4534(91)90749-o).

- [51] R. Prozorov, R. W. Giannetta, N. Kameda, T. Tamegai, J. A. Schlueter and P. Fournier, *Campbell penetration depth of a superconductor in the critical state*, Phys. Rev. B **67**, 184501 (2003), doi:[10.1103/PhysRevB.67.184501](https://doi.org/10.1103/PhysRevB.67.184501).
- [52] G. Ghigo et al., *Vortex dynamics in NbTi films at high frequency and high DC magnetic fields*, Sci. Rep. **13**, 9315 (2023), doi:[10.1038/s41598-023-36473-x](https://doi.org/10.1038/s41598-023-36473-x).
- [53] J. Srpcic, M. Ainslie, Y. Shi and J. Durrell, *The Campbell penetration depth in type-II superconductors*, In *7th international workshop on numerical modelling of high temperature superconductors*, Université de Lorraine, Nancy, France (2021).
- [54] S. Ghimire et al., *Creep-enhanced vortex pinning revealed through nonmonotonic relaxation of the Campbell length*, (arXiv preprint) doi:[10.48550/arXiv.2403.14891](https://doi.org/10.48550/arXiv.2403.14891).
- [55] R. T. Gordon, N. D. Zhigadlo, S. Weyeneth, S. Katrych and R. Prozorov, *Conventional superconductivity and hysteretic Campbell penetration depth in single crystals MgCNi₃*, Phys. Rev. B **87**, 094520 (2013), doi:[10.1103/PhysRevB.87.094520](https://doi.org/10.1103/PhysRevB.87.094520).
- [56] C. P. Bean, *Magnetization of hard superconductors*, Phys. Rev. Lett. **8**, 250 (1962), doi:[10.1103/PhysRevLett.8.250](https://doi.org/10.1103/PhysRevLett.8.250).
- [57] C. P. Bean, *Magnetization of high-field superconductors*, Rev. Mod. Phys. **36**, 31 (1964), doi:[10.1103/RevModPhys.36.31](https://doi.org/10.1103/RevModPhys.36.31).
- [58] G. Blatter, M. V. Feigel'man, V. B. Geshkenbein, A. I. Larkin and V. M. Vinokur, *Vortices in high-temperature superconductors*, Rev. Mod. Phys. **66**, 1125 (1994), doi:[10.1103/RevModPhys.66.1125](https://doi.org/10.1103/RevModPhys.66.1125).
- [59] R. Willa, V. B. Geshkenbein, R. Prozorov and G. Blatter, *Campbell response in type-II superconductors under strong pinning conditions*, Phys. Rev. Lett. **115**, 207001 (2015), doi:[10.1103/PhysRevLett.115.207001](https://doi.org/10.1103/PhysRevLett.115.207001).
- [60] R. Prozorov, V. G. Kogan, M. D. Vannette, S. L. Bud'ko and P. C. Canfield, *Radio-frequency magnetic response of vortex lattices undergoing structural transformations in superconducting borocarbide crystals*, Phys. Rev. B **76**, 094520 (2007), doi:[10.1103/PhysRevB.76.094520](https://doi.org/10.1103/PhysRevB.76.094520).